Polymer 50 (2009) 3269–3274

Contents lists available at ScienceDirect

Polymer

journal homepage: www.elsevier.com/locate/polymer

Influence of in-situ reaction on luminescent properties of samarium-complex/hydrogenated acrylonitrile-butadiene composites

Shipeng Wen [a], Xiaoping Zhang [a], Shui Hu [c], Liqun Zhang [a,b], Li Liu [a,b,*]

[a] Key Laboratory of Beijing City on Preparation and Processing of Novel Polymer Materials, Beijing University of Chemical Technology, Beijing 100029, China
[b] Key Laboratory for Nanomaterials, Ministry of Education, Beijing University of Chemical Technology, Beijing 100029, China
[c] Key Laboratory of Carbon Fiber and Functional Polymer, Ministry of Education, Beijing University of Chemical Technology, Beijing 100029, China

ARTICLE INFO

Article history:
Received 11 February 2009
Received in revised form
25 April 2009
Accepted 6 May 2009
Available online 14 May 2009

Keywords:
Fluorescence
Polymer
In-situ reaction

ABSTRACT

In this work, acrylato(1,10-phenanthroline)bis(2-thenoytrifluoroacetonato) samarium(III) [$Sm(TTA)_2(AA)(Phen)$] [Sm-AAPhen; TTA = 4,4,4-trifluoro-1-(2-thienyl)-1,3-butanedione, AA = acrylic acid, Phen = 1,10-phenanthroline] has been synthesized for the first time, which combines the good fluorescence property of $Sm(TTA)_3(Phen)$ and the reactivity of acrylic acid with radicals. The uncured composites were prepared by adding different amounts of the $Sm(TTA)_3(Phen)$ complex and a certain amount of peroxide into hydrogenated acrylonitrile-butadiene rubber (HNBR). The cured composites were prepared by vulcanizing the uncured composites at 160 °C under a pressure of 15 MPa for 20 min. Fourier Transform Infrared (FTIR) spectra show that the intensity of peaks assigned to reactive C=C bond decreases after the curing process, verifying that the in-situ reaction (including polymerization and grafting) of Sm-AAPhen initiated by peroxide radicals took place during the cross-linking of the HNBR matrix. Scanning electron microscopy (SEM) and Transmission electron microscopy (TEM) observations show that the dispersion dimension of the cured composite is far finer than that of the uncured composite. Wide-angle X-ray diffraction (WAXD) testing shows that the crystallinity of Sm-AAPhen in the composites was absent dramatically after the curing process, implying that most of crystalline Sm-AAPhen complex took part in the in-situ reaction and formed the non-crystalline poly(Sm-AAPhen). The dispersion phase of cured Sm-AAPhen/HNBR composites is composed of completely almost nanometer-sized poly(Sm-AAPhen) and few residual Sm-AAPhen particles with significantly reduced dimensions. The fluorescent intensity, lifetime and quantum yields of the cured composite are much higher than that of the uncured one with the same Sm-AAPhen content due to the in-situ reaction.

1. Introduction

In recent years, the rare-earth/polymer composites with luminescent properties have been widely studied for the possible applications in display [1], probes [2,3], and laser materials [4–7]. The organic rare-earth complex can emit strong fluorescence due to its special 4*f* electron structure of rare-earth and outstanding absorbing light ability of β-diketonate ligand [8–10]. The latest activity in the area of luminescent materials has been in developing unique rare-earth/polymer composites having not only the high lighting property but the good processing ability, chemical stability and mechanical strength [11]. Blending is a simple and effective way to get such composites. Zhang RJ et al. prepared Langmuir-Blodgett films (one or more monolayers of an organic material on a solid) containing $Sm(TTA)_3Phen$ (Phen = 1,10-phenanthroline) by using composite sub-phase and found both absorbance and relative fluorescence intensity increased linearly with the number of LB layers [12]. Zhang H et al. prepared rare-earth complex/polymer fibers prepared by electrospinning and observed that the thermal stability of photoluminescence in the composite fibers was considerably improved in comparison to the pure complex [13]. However, blending method can hardly achieve the fine dispersion and good interface interaction between the rare-earth complex and polymer matrix, leading the decrease of fluorescent properties of composites. Lin MJ et al. recently introduced an approach that combines the rare-earth complex with polymer by the bulk polymerization in an effort to prepare the $Sm(OPri)(TTA)_2$/PMMA photoluminescent material which showed a linear structure, and its luminescent strength was as high as that of $Sm(TTA)_3$/PMMA [14]. But as a consequence of the limitation of the polymerization caused by the effect of the steric clash resulting from the large

* Corresponding author. Key Laboratory for Nanomaterials, Ministry of Education, Beijing University of Chemical Technology, Beijing 100029, China. Tel.: +86 10 64434860; fax: +86 10 64433964.
E-mail address: liul2001cn@yahoo.com.cn (L. Liu).

0032-3861/$ – see front matter © 2009 Elsevier Ltd. All rights reserved.
doi:10.1016/j.polymer.2009.05.009

dimension of the rare-earth complex, it was found that the lower concentration of Sm(OPri)$(TTA)_2$ resulted in the lower fluorescent intensity of the material.

In our pervious study, we reported a new method of in-situ reaction process which can overcome the poor dispersion and weak interface interaction by blending and subsequent polymerization between the rare-earth complex with little concentration and polymer matrix. The work described the influence of in-situ reaction on the dispersion of rare-earth complex (gadolinium acrylate) and the interaction between them and the polymer matrix (natural rubber). The results illustrated that the self-polymerization of gadolinium acrylate did a good favor both in minishing aggregates of gadolinium acrylate and subsequently improved the X-ray shielding property and in reinforcing resultant composites [15]. This method was further successfully applied in fabricating another novel Eu-AAPhen/NBR composite with excellent fluorescence intensity [16].

In the present work, Sm$(TTA)_2$(AA)(Phen)][Sm-AAPhen; TTA = 4,4,4-trifluoro-1-(2-thienyl)-1,3-butanedione,AA = acrylic acid, Phen = 1,10-phenanthroline] was synthesized for the first time, which not only possessed the good fluorescence property for the ligand TTA and Phen whose triplet states could well match the $^4G_{5/2}$ emitting states of Sm^{3+}, but also could be initialized by radicals due to the existence of the acrylic acid (AA). Various amounts of this reactive complex were mechanically mixed with hydrogenated acrylonitrile-butadiene rubber (HNBR) by the similar way as described in Ref. [16]. HNBR was chosen as the polymer matrix because of its strong polarity and high shearing viscosity which helped initial dispersion of the rare-earth complex during filling them into the polymer. Even though HNBR has more degree of saturation compared with nitrile-butadiene used as polymer matrix as described in our previous work, the in-situ reaction is also feasible to occur in the presence of the peroxide in such saturated polymer at high temperature that has been demonstrated by a few reports [17,18].

2. Experimental section

2.1. Materials

Samarium oxide (Sm_2O_3, 99.99%) was supplied by Shanghai Yue Long Chemicals (China). Hydrogenated acrylonitrile-butadiene rubber (HNBR, 41 wt% CN, $M_w \sim 50 \times 10^4$ g mol^{-1}) was purchased from Bayer Co. 2-Thenoytrifluoroacetonatone (TTA-4,4,4-trifluoro-1-(2-thienyl)-1,3-butanedione), 1,10-phenanthroline (Phen), acrylic acid (AA), and other chemicals are commercial products.

2.2. Synthesis of Sm$(TTA)_2$(AA)(Phen) complex

Ethanol (30 mL), 2-thenoyltrifluoroacetone (0.1 mol), and acrylic acid (0.05 mol) were added to a 250 mL side-arm flask. The system was stirred for 20 min and then 1,10-phenanthroline (0.05 mol) and $SmCl_3$ (0.05 mol) were added to the flask. The reaction mixture was heated and magnetic stirred with the speed of 20 rpm at 60 °C for 5 h. After that the mixture was cooled to room temperature. Then, triethylamine was added to adjust the pH of the mixture to 5–6. Then the precipitate was filtered and washed with ethanol for several times and dried at 80 °C in a vacuum oven. The product of the complex was characterized by elementary analysis as Sm$(TTA)_2$(AA)(Phen). Product yield: 80%. Anal. calcd. C: 44.00%, H: 2.48%, N: 3.31%, Found: C: 43.38%, H: 2.12%, N: 3.12%.

2.3. Preparation of Sm-AAPhen/HNBR composites

The composite with 2 wt% Sm-AAPhen content in HNBR matrix was prepared as follows. First, 48 g of the HNBR, 2 g 2,5-dimethyl 2,5-bis (*t*-butyl peroxy) hexyne (peroxide D25) and 1.02 g Sm-AAPhen complex were mixed in a mixer (Haake, rheomix 610, Ger.) at 50 °C with 80 rpm (revolutions per minute) for 15 min to get the compound (uncured composites); then the compound was molded and vulcanized at 160 °C under a pressure of 15 MPa for 20 min to get the cured composites with a thickness of 1 mm. Other composites with different Sm-AAPhen complex contents (5 wt%, 8 wt%, 12 wt% and 15 wt%) were prepared according to the same procedure.

2.4. Characterization

Elemental analysis of the pure Sm-AAPhen complex was carried out by using a Perkin–Elmer 2400 CHN–O Rapid instrument. The Fourier Transform Infrared (FTIR) spectra of the samples (pure Sm-AAPhen, uncured and cured composites) were recorded at a resolution of 1 cm^{-1} on Bruker Tensor 27 Spectrometer. The X-ray diffraction analysis of the samples was performed by a D/max2500 diffractometer with CuKα radiation (40 kV and 20 mA, $\lambda = 0.154$ nm). The morphologies of Sm$(TTA)_2$(AA)(Phen) and Sm$(TTA)_2$(AA)(Phen)/HNBR composites were observed by using scanning electron micrographs (SEM; Cambridge S-250-III, 20 kV.) and transmission electron microscopy (TEM; Hitachi H-800-1). The fracture surfaces of composites were obtained by breaking the long strip samples in liquid nitrogen. Each sample was covered by gold vapor under vacuum before SEM observation. The thin sections for TEM observation were cut by microtome under −100 °C and collected on the cooper grids. The fluorescent spectra of the samples were recorded with a Hitachi F-4500 Fluorescent spectrometer equipped with a 450 W Xenon lamp as the excitation source with excitation and emission slit width of 2.5 nm. The fluorescent lifetime of excited state (646 nm) was measured by the steady-state and lifetime spectrofluorometer (FL3-2-IHR221-NIR-TCSPC, HORIBA Jobin Yvon Inc) equipped with an Nd^{3+}:YAG (yttrium aluminum garnet) pulse laser and excited by 376 nm. The fluorescent yields of the composites were obtained by the integral sphere in the FluoroMax-4 Spectrofluorometer (HORIBA Jobin Yvon Inc) and excited by 376 nm.

3. Results and discussion

For verifying the in-situ reaction in the curing process of Sm-AAPhen/HNBR composites, the IR spectra (band 1800–650 cm^{-1}) of Sm-AAPhen/HNBR composites are shown in Fig. 1. In the spectrum of Sm-AAPhen complex (Fig. 1A), the bands at 1641 cm^{-1} are assigned to C=O vibration of TTA. The bands at 1517 cm^{-1} are assigned to the C=N stretching vibration of Phen. The stretching vibration (COO^-) peaks of AA appear at 1426 and 1540 cm^{-1}, while the reactive C=C stretching vibration peak of AA appears at 1574 cm^{-1}. In the spectrum of uncured composites (Fig. 1B), the

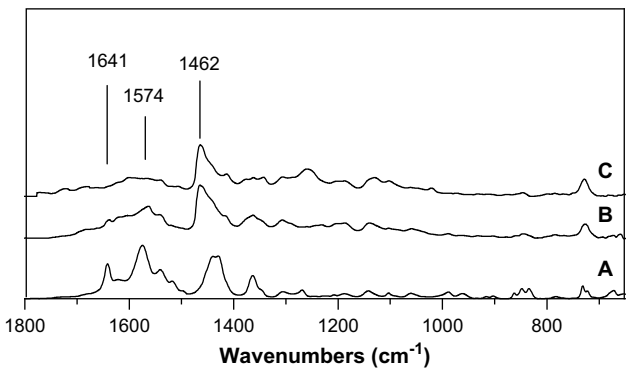

Fig. 1. FTIR spectra of (A) Sm-AAPhen, (B) uncured and (C) cured Sm-AAPhen/HNBR composites containing 15 wt% Sm-AAPhen.

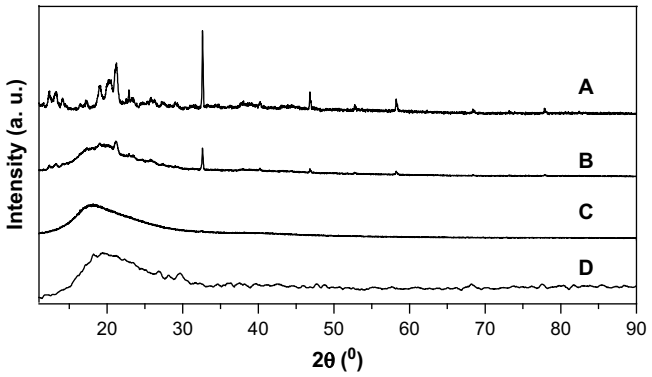

Fig. 2. XRD patterns of (A) the original Sm-AAPhen, (B) uncured and (C) cured Sm-AAPhen/HNBR composites containing 15 wt% Sm-AAPhen, (D) cured pure HNBR.

C═C peak of AA can be still observed at 1574 cm^{-1}, although the intensity of peak decreases due to the concentration effect. The bands at 1462 cm^{-1} are assigned to the C–H scissor vibration of HNBR. In the spectrum of cured composites (Fig. 1C), the intensity of C–H vibration at 1462 cm^{-1} of HNBR does not change after curing process. However, the band intensity at 1574 cm^{-1} decreases significantly after the curing process, showing the decrease of the content of reactive double bonds. This reveals that most Sm-AAPhen complex have participated in the in-situ reaction in the HNBR matrix during the curing process.

In order to further verify the occurrence of the in-situ reaction during the curing process, wide-angle X-ray diffraction (WAXD) test is used to prove the structural change of Sm-AAPhen complex in both uncured and cured composites. As shown in Fig. 2A, the diffraction peaks of the original Sm-AAPhen complex are quite strong, indicating the crystal of Sm-AAPhen complex. In the curve of Fig. 2B, the broad scattering ($2\theta = 18^{\circ}$) is likely attributed to the amorphous nature of HNBR matrix, which is shown in Fig. 2D. The characteristic crystal diffraction of the Sm-AAPhen complex ($2\theta = 23^{\circ}$ and 33°) can also be obviously observed in the uncured composite. However, the intensities of these characteristic peaks become lower due to the concentration effect. After curing process, as shown in Fig. 2C, the characteristic crystal diffraction of the Sm-AAPhen complex almost disappears. It deserves to be noted that the crystal transformation of Sm-AAPhen complex during the curing process can hardly take place, since the curing temperature (160 °C) is much lower than the melting point of Sm-AAPhen complex (261 °C). The WAXD results strongly support the fact that most of crystalline Sm-AAPhen complex took part in the in-situ reaction and formed the non-crystalline poly(Sm-AAPhen).

Combined the above characterization with our previous basic research on the in-situ reactions [15,16,19], the chemical reaction mechanism during the curing process is shown in Fig. 3. The peroxide is firstly decomposed to form radicals by heating, inducing the reaction of the double bonds of the Sm-AAPhen monomer and rubber chains. Consequently, the Sm-AAPhen radicals and the rubber radicals are formed respectively. The former initiates its monomer and gives chain growth of poly(Sm-AAPhen) until the chain radicals are terminated by reaction with other radicals. If they are terminated by other poly(Sm-AAPhen) radicals, the separated poly(Sm-AAPhen) molecules are subsequently formed. If they are terminated by rubber chain radicals, the grafted poly(Sm-AAPhen) with rubber chain obtains. Simultaneously, reactions between rubber chain radicals result in the rubber matrix cross-linking by covalent bonds.

The scanning electron microscopy (SEM) image in Fig. 4A shows the morphology of the original Sm-AAPhen particles. The average size of these particles is about 4 μm with relatively regular shape. There are also some aggregates with the size about 10–20 μm formed by the original Sm-AAPhen particles. In the SEM image of the uncured Sm-AAPhen/HNBR composite (Fig. 4B), the light phase represents the dispersed Sm-AAPhen complex particles and/or their aggregates with dimension about 2–4 μm which has been decreased considerably comparing with that of the original Sm-AAPhen complex particles because of the high mechanical shearing and grinding effects during the mixing procedure. After curing, the size of the dispersed particles in HNBR was further decreased and the largest Sm-AAPhen complex particle size is only about 1 μm (Fig. 4C). It indicates significantly that the in-situ reaction has a great effect on improving the Sm-AAPhen complex's dispersion in the curing process.

Transmission electron microscopy (TEM) measurements were conducted to reveal how efficiently the Sm-AAPhen complex

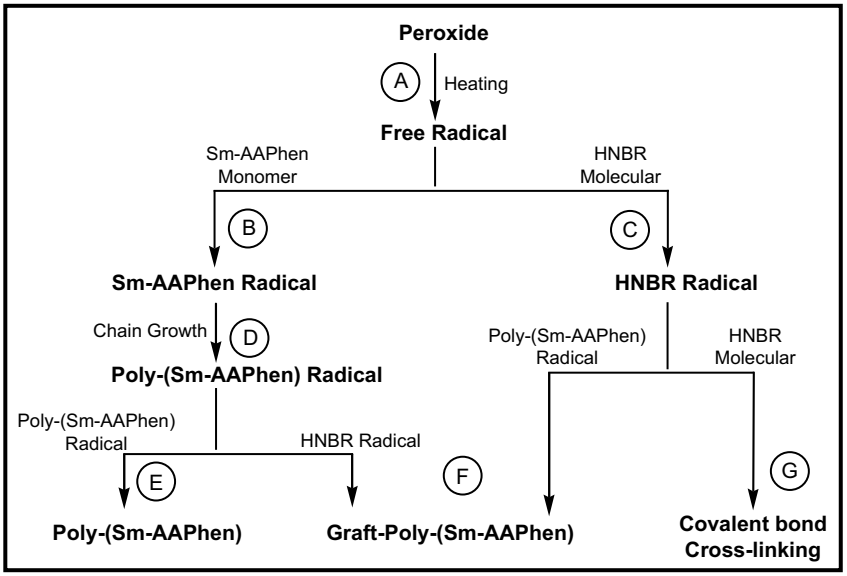

Fig. 3. In-situ reactions in the composites during curing: (A) Decomposing of peroxide by heating. (B) Sm-AAPhen is initiated to form Sm-AAPhen radical. (C) HNBR is initiated to form HNBR radical. (D) Chain growth of poly(Sm-AAPhen). (E) Termination of poly(Sm-AAPhen) chain. (F) Graft reaction between HNBR and poly(Sm-AAPhen). (G) Generation of covalent crosslinks.

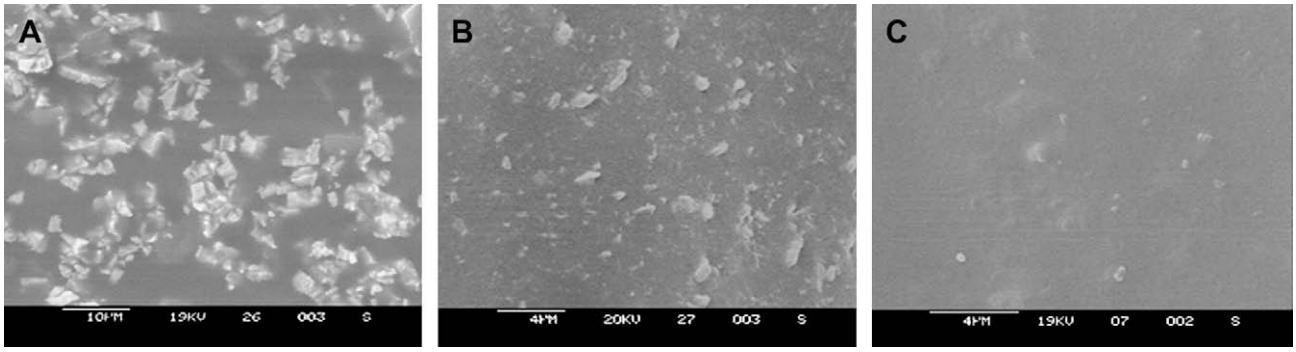

Fig. 4. SEM photos of (A) Sm-AAPhen original particles (B) uncured and (C) cured Sm-AAPhen/HNBR composites containing 15 wt% Sm-AAPhen.

particles were dispersed in the composite. A typical image of the composite is depicted in Fig. 5. The average sizes of Sm-AAPhen complex particles are estimated to be around 200–500 nm, although some big aggregates are seen in Fig. 5. The statistic size distribution of particles (Fig. 6) shows that the particles with the size of 27–104.2 nm accounts for 53.58% of the total particles in the cured composites. It's suggested that such fine dispersion of the particles in the composite resulted from the in-situ reaction [16]. Combining with the analysis of XRD and FTIR data, the poly(Sm-AAPhen) molecules aggregated to form almost nanometer-sized dispersion particles in the curing process. Meantime, the particle size of Sm-AAPhen reduced gradually due to the consumption of substantial Sm-AAPhen molecules during the in-situ reaction process. Therefore, few micrometer-sized particles observed in Fig. 4C should be the residual of Sm-AAPhen particles.

The excitation and emission spectra of the Sm-AAPhen are shown in Fig. 7. The excitation spectrum (Fig. 6A) of the Sm-AAPhen complex shows a broad band covering the entire 200–400 nm regions. The broad excitation band is assigned to the π–π^* electron transition of the ligands. In the emission spectrum of Sm-AAPhen (Fig. 7B), there are three characteristic fluorescence emission bands assigned with Sm^{3+} ions, which are the characteristic peaks of the $^4G_{5/2} \rightarrow {}^6H_J$ transitions ($J = 5/2,7/2,9/2$) [20]. The peak at 564 nm corresponds to the $^4G_{5/2} \rightarrow {}^6H_{5/2}$ transition of Sm^{3+} ions, the two peaks at 603 nm and 610 nm correspond to the $^4G_{5/2} \rightarrow {}^6H_{7/2}$ transition of Sm^{3+} ions, and the strongest peak at 646 nm corresponds to the $^4G_{5/2} \rightarrow {}^6H_{9/2}$ hypersensitive transition of Sm^{3+} ions.

Fig. 8 shows the emission spectra of uncured and cured Sm-AAPhen/HNBR composites with different content of Sm-AAPhen. It can be seen that both cured and uncured composites (Fig. 8A and B) possess the similar characteristic emission peaks of original Sm-AAPhen. The fluorescence intensity around 646 nm of uncured and cured composites increases with the growth of Sm-AAPhen content. Additionally, when the emission intensities (646 nm) of the composites are plotted as a function of weight concentration of Sm-AAPhen, as shown in Fig. 8C, it is obvious to observe that the fluorescent intensities of cured composites are twenty percent higher than that of uncured composites. The photoluminescence quantum efficiencies of the cured and uncured samples containing 15 wt% Sm-AAPhen measured by the integrating sphere method were 0.7% and 0.3%, respectively. It indicates that in-situ reaction in

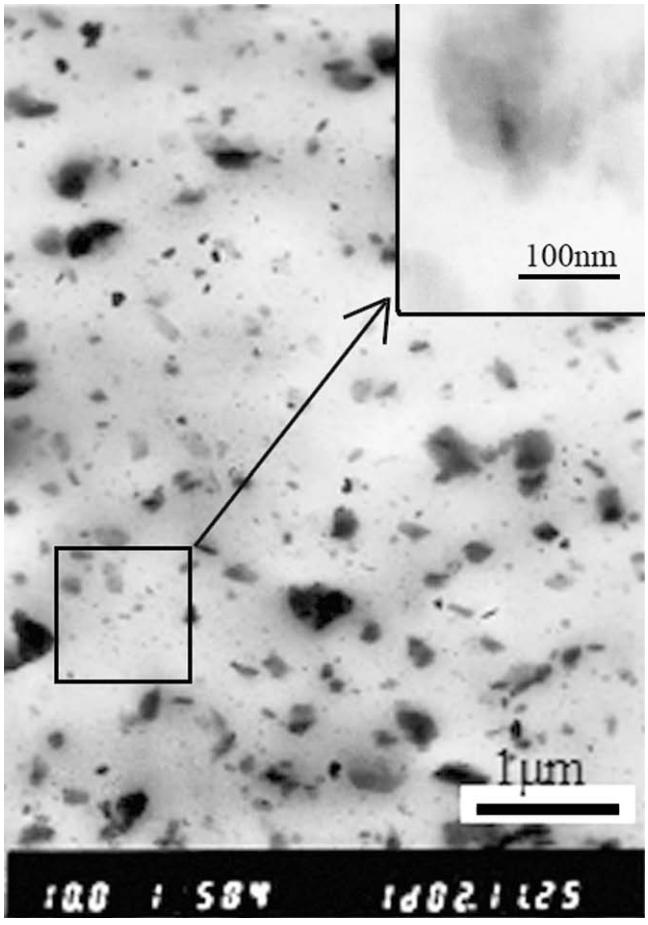

Fig. 5. TEM images of the cured Sm-AAPhen/HNBR composites containing 15 wt% Sm-AAPhen.

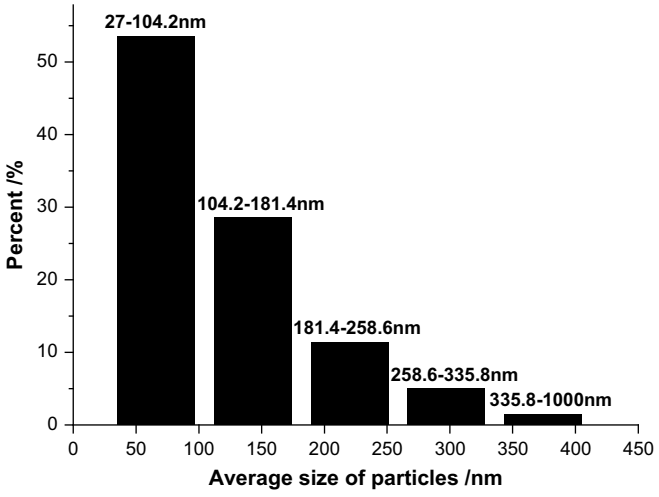

Fig. 6. Statistic size distribution of particles in the cured composites.

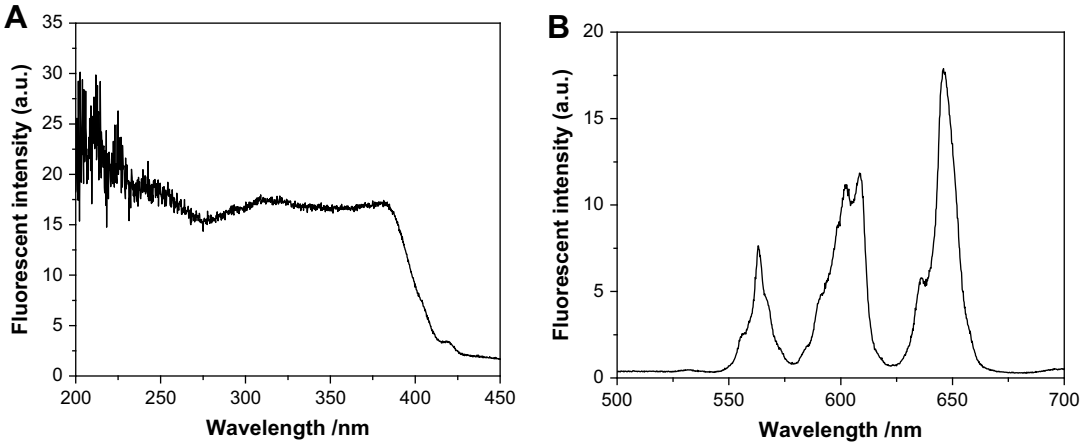

Fig. 7. Excitation and emission of Sm-AAPhen (Split Ex/Em = 2.0/2.0 nm): (A) excitation spectrum (λ_{em} = 612 nm) and (B) emission spectrum (λ_{ex} = 385 nm).

the cured composites has effect on improving both the fluorescent intensity and the quantum yields of composites. Combining with the SEM and TEM observations (Figs. 4 and 5), it suggests that the Sm-complex particles are more finely and uniformly dispersed in the cured composites other than the uncured ones, resulting in a much larger surface area of Sm-complex particles in the cured composites with the same content of Sm^{3+}. Therefore, such a fine dispersion level would lead to a higher fraction of Sm^{3+} in dispersed particles that are easily irradiated by the excitation light and emit fluorescence.

Nevertheless, the nonlinear relationship between fluorescent intensity and rare-earth content is also observed in this present work, suggesting the consequence of the negative affection of in-situ reaction on fluorescent emission. As similar to the discussion in our previous work about Eu^{3+} [16], in this work, the formation of aggregates within poly(Sm-AAPhen) particles where rare-earth ions are close together will theoretically lead to more energy transfer between neighboring Sm^{3+} centers, which depresses the quantum efficiency of Sm^{3+} to some extent. The competition between positive factors and negative ones would finally determine

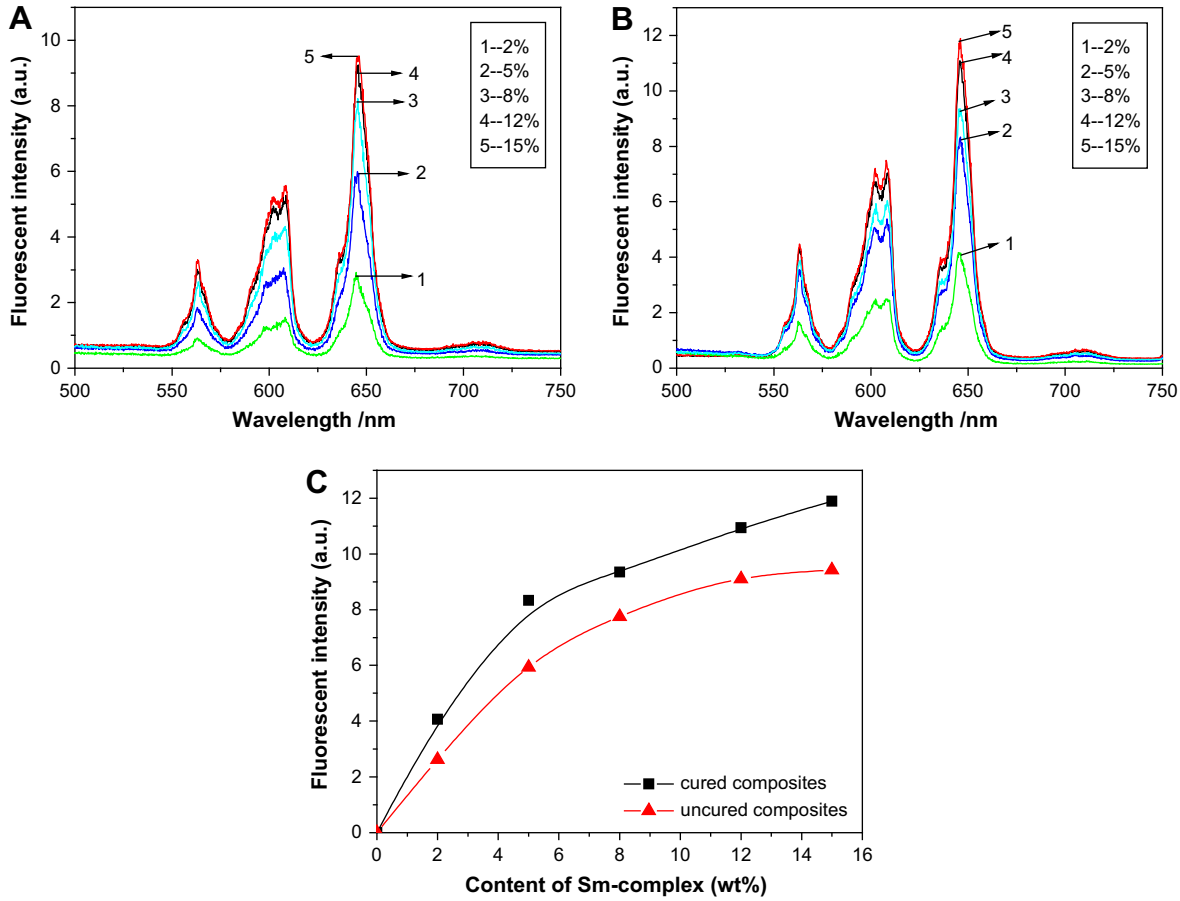

Fig. 8. Fluorescent emission spectra (λ_{ex} = 385 nm) of (A) uncured and (B) cured Sm-AAPhen/HNBR composites with different concentrations of Sm-AAPhen. (C) A plot of the emission-intensity variation at 646 nm against rare-earth complex content for uncured and cured composites.

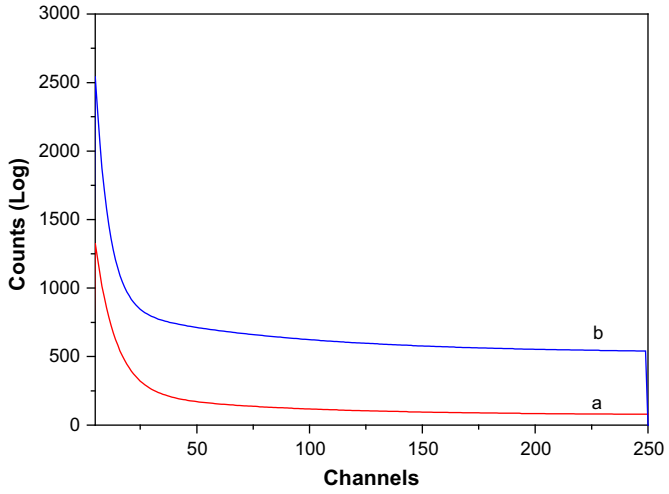

Fig. 9. Fluorescent decay curves of (a) uncured composites (Fitted lifetime $T_1 = 7.82$, $T_2 = 1.02$) and (b) cured composites (Fitted lifetime $T_1 = 17.3$, $T_2 = 1.37$) containing 15 wt% Sm-AAPhen complex.

the quantum yields of the cured composites, and the degree of such deviation of the relationship between fluorescent intensity and Sm^{3+} content. Obviously, our results show that the positive factors caused by the formation of fine poly(Sm-AAPhen) particles by in-situ reaction are more significant than the negative ones.

The fluorescence lifetimes of Sm-AAPhen/HNBR composites were also investigated, as shown in Fig. 9. The decay curve of the composites can be fitted by bi-exponential functions, revealing there are two chemical microenvironments around Sm^{3+} ions [21]. The ratio of two fitted lifetime values (T_1/T_2) can be applied in showing the asymmetry of two chemical microenvironments around Sm^{3+} ions in the composites. It is noteworthy that the T_1/T_2 value (12.63) of the cured composite is significantly higher than that (7.67) of the uncured composite, indicating the original chemical microenvironments around Sm^{3+} ions changed. The site symmetry of Sm^{3+} ions became lower in the cured composite resulting from the formation of the poly(Sm-AAPhen) and the chemical interaction occurred between Sm-AAPhen and HNBR matrix during the in-situ reaction. The high asymmetry of chemical microenvironments would sensitize the ability of energy transfer of Sm^{3+} ions in the composites and improve the quantum yields of the composites [22–25].

4. Conclusions

In this work, we have prepared Sm-AAPhen/HNBR composites with the characteristic Sm^{3+} fluorescence and high fluorescent property by the in-situ reaction method. Microstructure characterization and the analysis of fluorescent property of the composite shows the fine dispersion of poly(Sm-AAPhen) particles in the cured composites and chemical interface between the Sm-AAPhen and HNBR matrix, which are the main reasons for the good luminescence of the Sm-AAPhen/HNBR composites. Compared with the uncured composites, the cured composites exhibit high fluorescent intensity, quantum yields and long fluorescent lifetime.

Acknowledgments

Project supported by the National Natural Science Foundation of China, the China Energy Conservation Investment Corporation (50173004 and 50503002), the Beijing New Star Project (2003A11), the National High-Tech Research Developing Foundation (863,2003AA324030), Beijing Municipal Commission of Education (JD100100403), National Key Project of Scientific and Technical Supporting Programs Funded by Ministry of Science & Technology of China (NO. 2006BAE03B), Program for New Century Excellent Talents in University (NCET) and Program for Changjiang Scholars and Innovative Research Team in University (PCSIRT, IRT0807).

References

[1] Thomas HN, Cees R. Angew Chem Int Ed 1998;37(22):3084–103.
[2] Hassey R, Swain EJ, Hammer NI, Venkataraman D, Barnes MD. Science 2006;314(5804):1437–9.
[3] Alpha B, Balzani V, Lehn JM, Perathoner S, Sabbatini N. Angew Chem Int Ed 1987;26(12):1266–7.
[4] Robinson MR, Ostrowski JC, Bazan GC, McGehee MD. Adv Mater 2003; 15(18):1547–51.
[5] Abdullah M, Morimoto T, Okuyama K. Adv Funct Mater 2003;13(10):800–4.
[6] Yang CY, Srdanov V, Robinson MR, Bazan GC, Heeger AJ. Adv Mater 2002; 14:980–3.
[7] Yokoyama H. Science 1992;256(5053):66–70.
[8] Masatsugu M, Hiroyuki O. J Electroanal Chem 1998;452:141–9.
[9] Dong D, Jiang S, Men Y, Ji X, Jiang B. Adv Mater 2000;12:646–9.
[10] McGehee MD, Bergstedt T, Zhang C, Saab AP, O'Regan MB, Bazan GC, et al. Adv Mater 1999;11:1349–54.
[11] Moleski R, Stathatos E, Bekiari V, Lianos P. Thin Solid Films 2002;416:279–83.
[12] Zhang RJ, Liu HG, Zhang CR, Yang KZ, Zhu GY, Zhang HW. Thin Solid Films 1997;302:223–30.
[13] Zhang H, Song HW, Yu HQ, Li SW, Bai X, Pan GH, et al. Appl Phys Lett 2007;90(10):103103.
[14] Lin MJ, Wang W, Zhang WG. Acta Polymerica Sinica 2006;8:1013–8.
[15] Liu L, He L, Yang C, Zhang W, Jin RG, Zhang LQ. Macromol Rapid Commun 2004;25:1197–202.
[16] Liu L, Lu YL, He Lei, Zhang W, Yang C, Liu YD, et al. Adv Funct Mater 2005; 15(2):309–14.
[17] Wang YH, Peng ZL, Zhang Y, Zhang YX. China Rubber Industry 2006;53(1):10–5.
[18] Wang YH, Peng ZL, Zhang Y, Zhang YX. China Synthetic Rubber Industry 2005; 28(3):1205–10.
[19] Lu YL, Liu L, Shen DY, Yang C, Zhang LQ. Polym Int 2004;53:802–8.
[20] Chen XY, Jensen MP, Liu GK. J Phys Chem B 2005;109:13991–9.
[21] Liu HG, Lee YI, Park S, Jang K, Kim SS. J Lumin 2004;110:11–6.
[22] Julian B, Beltra'n H, Cordoncillo E, Escribano P, Viana B, Sanchez C. J Sol–Gel Sci Technol 2003;26:977–80.
[23] Chowdhury PS, Saha S, Patra A. Solid State Commun 2004;131:785–8.
[24] Legendziewicz J, Oczko G, Wiglusz R, Amirkhanov V. J Alloy Compd 2001;323–324:792–9.
[25] Huskowska E, Turowska-Tyrk I, Legendziewicz J, Glowiak T. J Alloy Compd 1998;275–277:852–8.